Facile synthesis of high-performance $Ni(OH)_2$/expanded graphite electrodes for asymmetric supercapacitors

Jiawei Yuan[1,2], Shuihua Tang[1,2*], Zhentao Zhu[1,2], Xiaolong Qin[1,2], Renjie Qu[1,2], Yuxiao Deng[1,2], Lingshan Wu[1,2], Jie Li [1,2]

[1] State Key Lab of Oil and Gas Reservoir Geology & Exploitation, Southwest Petroleum University, Chengdu 610500, PR China

[2] School of Materials Science and Engineering, Southwest Petroleum University, Chengdu 610500, PR China

* Corresponding author. Tel/Fax: +86-2883032879. Email address: spraytang@hotmail.com (S. Tang).

Abstract

Cost-effectively commercial expanded graphite (EG) was used as a raw material, and a facile *in-situ* electrodeposited method has been adopted to synthesize a layered $Ni(OH)_2$/EG composite electrode in a N,N-dimethylformamide-water system. The structure composed of expanded graphite sheets, $Ni(OH)_2$ nanoparticles and carbon nanotubes can be observed by Scanning electron microscopy, which not only effectively restraint the restacking of EG sheets but also prevents the aggregation of nickel hydroxide particles. The obtained electrode shows better capacitive performances with satisfactory initial specific capacitance (1719.5 F/g at 1 A/g), remarkable rate capability (1181.3 F/g at 10 A/g) based on a total mass loading of 5.0 mg/cm^2. Furthermore, an asymmetric supercapacitor (ASC) device, with a negative electrode of commercial activated carbon (AC) and a positive electrode of as-prepared composite, delivers a prominent energy density of 32.3 Wh/kg at power density 504.7 W/kg, long cycling life with 79% original capacitance after 1000 cycles. Consequently, the facile synthesized high-performance $Ni(OH)_2$/expanded graphite electrodes are expected to be applied for energy

storage/conversion.

Keywords: Expanded graphite; Electrodeposition; $Ni(OH)_2$/EG composite; Supercapacitors

1. Introduction

Recently, severe environmental issues and energy depletion have pushed human being to develop green and sustainable energy storage/conversion devices [1-3]. As a promising candidate, Supercapacitors (SCs) have received significant attention owing to their excellent cycling lifespan, high power density, fast charge/discharge rate, environmental benignity and safe usage [4-7]. However, low energy density and high costs restrict their wide applications in energy storage. Developing novel electrode materials which have a high specific capacitance and low price to increase device capacitance or assembling asymmetric supercapacitor (ASC) to broaden the cell voltage is effective strategy to address this problem on the basis of the equation of energy density (E) $E = {}^{1}/_{2}\,CV^{2}$ [8].

Nickel hydroxide with well-defined redox activity, desirable theoretical capacitance and environmental friendliness has been extensively investigated nowadays [9-11]. Unfortunately, the poor electronic conductivity (10^{-17} S/cm) of nickel hydroxides hinders electron transfer and reduces the efficiency of redox reactions, leading to low power densities and rate capabilities [12]. Thus, adding high conductive carbon materials can greatly enhance the capacitive performances of nickel hydroxide. Activated carbon (AC) [13-15], carbon nanotubes (CNTs) [16-19], grapheme (GR) [20-25], expanded graphite (EG) [26] and Vulcan XC-72 [27] have been widely investigated. Besides, tremendous works have been done to fabricate aqueous electrolyte-based ASC, with nickel hydroxide-carbon composites as the positive electrode and commercial activated carbon (AC) as the negative electrode material (denoted as AC//$Ni(OH)_2$/C). For example, AC//$Ni(OH)_2$/GR [28], AC//$Ni(OH)_2$/CNT/AC [29], AC//$Ni(OH)_2$/$Co(OH)_2$/GR [30], AC//$Ni(OH)_2$/CNT [17]. These ASCs exhibits a high energy density.

EG has been investigated owing to its unique properties in terms of excellent electrical conductivity, good chemical stability, cheap price, relatively wider interlayer spacing and larger specific surface area as compared to graphite [31]. Guo et al [32] prepared AC/EG composite by a novel supersonic wave shocking method, the largest specific capacitance (*Cs*) can reach to 305 F/g at 1 mA charging current. Besides, Xu et al [26] prepared NiO/EG composite via a chemical precipitation method, the *Cs* is 510 F/g at 0.1 A/g. Nevertheless, poor capacitive performances of electrode material prepared from EG are the most pressing problem which needs to be solved.

In this work, low cost EG was used as carbon material, a facile *in-situ* electrodeposited method has been adopted to obtain a layered nickel hydroxide/EG composite electrode, achieving a high initial *Cs* (1719.5 F/g at 1 A/g), remarkable rate capability (1181.3 F/g at 10 A /g). These results indicate that as-prepared electrode have better capacitive performances than other EG-based electrodes. Moreover, an ASC device, with a negative electrode of commercial activated carbon (AC) and a positive electrode of as-prepared composite, was assembled and its electrochemical performances were investigated.

2. Experimental

2.1 Preparation of materials

Firstly, nickel foam (10 mm × 10 mm, Changsha Liyuan New Material Co., Ltd) was ultrasonically cleaned with an acetone, deionized water and ethanol for 30 min, then dried a vacuum oven. Secondly, EG/CNTs slurry was obtained by mixing 85 wt% EG, 10 wt% CNTs (Chengdu Organic chemicals Co., Ltd, as a conductive agent) and 5 wt% Nafion$^{\bigcirc,R}$ solution (Du Pont Company, as a binder). The slurry was ultrasonically stirred until a homogeneous dispersion was obtained. Then the slurry was dropped uniformly onto the Ni foam substrate, controlling a mass loading of EG, CNTs and Nafion solution was 2.0 mg/cm^2, and dried at 70 ºC overnight. Finally, the deposition of nickel hydroxide was

conducted in a three-electrode cell, which consisted of a nickel foam plate (20 mm× 20 mm), counter electrode, saturated calomel electrode (SCE) reference electrode and as-prepared EG working electrode, a 302N Autolab potentiostat (Metrohm Holland) was used as power supplies. The potential was fixed at -1.1 V vs. SCE electrode and electrolyte solution was 0.1 M $Ni(NO_3)_2 \cdot 6H_2O$ in a 1:10 (v/v) H_2O/DMF mixed solvent. The electrodeposition was conducted under both potentiostatic and room temperature. After deposition for 12 min, the as-prepared electrode was rinsed with water before being dried. Finally, the mass loading of deposition production was 3.0 mg/cm^2.

The preparation of $Ni(OH)_2$ nanoparticles include an electrochemical and a chemical process, which can be described in following steps [33]:

$$NO_3^- + 7\ H_2O + 8\ e^- \rightarrow NH_4^+ + 10\ OH^-$$

$$2OH^- + Ni^{2+} \rightarrow Ni(OH)_2$$

2.2 Characterizations

The prepared materials was characterized using Philips X' pert pro MPD X-ray diffraction (XRD, Cu, k=0.15406 nm). The morphology and microstructures of EG and prepared electrode were observed on Zeiss scanning electron microscope (SEM, EVO MA15), Hitachi Field emission scanning electron microscope (FESEM, JSM-7500F/X-MAX50). The typical morphologies of prepared material were obtained from Zeiss Transmission electron microscope (TEM, LiBRA 200FE). Infrared spectrum was obtained on a Fourier transform infrared spectrometer (FT-IR, Nicolet 6700).

2.3 Assembly of asymmetric supercapacitor (ASC) device

An AC//$Ni(OH)_2$/EG device, with a negative electrode of commercial activated carbon (AC) and a positive electrode of as-prepared composite, nonwoven fabrics (NKK company, Japan) as diaphragm, was fabricated in a two-electrode configuration. The AC electrode was obtained by mixing 80 wt% the

commercial AC, 10 wt% CNTs and 5 wt% polytetrafluoroethylene (PTFE) in ethanol and brushed onto Ni foam substrate (Φ=14 mm) before being dried at 80 ºC. Then the electrode materials and diaphragm were soaked in 6 M KOH electrolyte overnight before assembly.

2.4 Electrochemical studies

Electrochemical studies of as-prepared composite and AC electrode were carried out on a 302N Autolab potentiostat in a three-electrode system, with as-prepared composite as working electrode, Pt coil as counter electrode and Hg/HgO as reference electrode. 6 M KOH was used as electrolyte. The *Cs* can be estimated by cyclic voltammetry (CV) or galvanostatic charge-discharge (GCD) curves based on the equation (1) and (2), respectively:

$$Cs = {\int IdV}/{2m\vartheta\Delta V} \qquad (1) \qquad\qquad Cs = I \times \Delta t/m \times \Delta V \qquad (2)$$

Where *Cs* (F/g), *I* (A), *m* (g), Δt (s) represents the specific capacitance, respond current, mass of the electrode materials and discharge time, respectively. ϑ (mV/s) indicates the scan rate and ΔV (V) represents potential window.

The as-assembled ASC device was measured using a two-electrode mode. Electrochemical impedance spectroscopy (EIS) was carried out by applying 5 mV perturbation amplitude versus the open circuit, the frequency was choose from 100 kHz to 0.01 Hz. The energy density (*E*) was estimated based on equation (3) and power density (*P*) was obtained by the formula (4) respectively:

$$E = {1}/{2}\, Cs \times V^2 \qquad (3)$$

$$P = {E}/{t} \qquad (4)$$

Where *V* (V), *Cs* (F/g), *t* (s) represents the voltage window, specific capacitance of total cell and discharge time, respectively.

3. Results and discussion

XRD pattern of composite by peeling off the obtained electrode is presented in Fig. 1a. Except for three diffraction peaks associated with the nickel foam substrate and one diffraction peak for graphite, no characteristic peaks can be observed form the pattern. It is speculated that the prepared nickel hydroxide particles is amorphous. Besides, a broad and diffused halo ring associated with nickel hydroxide can be found from selected-area electron-diffraction pattern (Fig. 4d inset). The results further demonstrate that nickel hydroxide deposits are an amorphous morphology. The energy dispersive X-ray spectroscope (EDS) spectra (Fig. 1b) show that O, C, and Ni elements are present in the composites.

The FT-IR spectrum of the obtained composites shows the characteristic band at 3410 and 3170 cm^{-1} in Fig. 2 corresponding to inter-lamellar water and the hydroxyl groups, respectively [34]. The broad band around 3140 and 1623 cm^{-1} are assigned to the N-H stretching vibration and δ-H_2O vibration of the water molecule. The band at 1400 cm^{-1} is the characteristic band of interlayer nitrate anion [35]. The band at 1160 cm^{-1} is attributed to the *v*-N-H vibration. Its existence could be due to the DMF in solution. Furthermore, there are two bands at the low wavenumber, corresponding to the Ni-O-H bending vibration at 616 cm^{-1} and Ni-O stretching vibration at 450 cm^{-1}, respectively [36]. These results show that the nickel hydroxide is present in the prepared composite.

The morphologies and structures of EG and obtained electrode are observed by SEM and TEM. The EG sheets have a layered structure and wide interlayer spacing from SEM image (Fig. 3), the nickel hydroxide nanoparticles can be easily intercalated into the graphite layer by electrochemical deposition. As seen in Fig. 4a~b, the composites exhibits a layered structure, nickel hydroxide particles intercalated into the graphite layer and deposited on the surface of graphite sheets. The embedded nickel hydroxide nanoparticles expand interlayer spacing and create some pore structures, which is beneficial to the

infiltration of electrolyte. The TEM (Fig. 4c) displays that the EG sheets are thin and possess a number of wrinkles, acting as apposite materials to support the nickel hydroxide particles. From Fig. 4d, it can be see that most of nickel hydroxide nanoparticles have an average diameter of 35 nm and homogeneously anchored on EG interlayer. In summary, the XRD, SAED, EDS, FT-IR, SEM and TEM measurements indicate that deposits are amorphous nickel hydroxide nanoparticles. However, the particles exhibit a relatively larger particle size, resulting in a poor rate performance and cycle life. Further research will be done to obtain smaller nickel hydroxide nanoparticles.

3.2 Electrochemical performances of electrode materials

In order to certify high electrochemical performances of as-prepared electrodes, the capacitances are investigated using CV and GCD tests. Fig. 5a displays CV curves of nickel hydroxide/EG composite electrode with various scanning rates (2 ~ 20 mV/s), potential window is fixed from 0.1 V to 0.55 V. It can be observed that all CV curves show a couple of clear redox peaks, which derives from the following faradic reaction:

$$Ni(OH)_2 + OH^- \leftrightarrow NiOOH + H_2O + e^-$$

Demonstrating that the charge storage mainly derives from the pesudocapacitance resulted from Faradaic reaction. As noted, the anodic peak shows a remarkable diffusion tail at 20 mV/s. The result indicates a relatively lower charge-transfer process [37]. Besides, as shown in Fig. 5b, the electrode displays a well-defined discharge potential plateau from 1 A/g to 10 A/g. Furthermore, the plots of the *Cs* versus current density (Fig. 5c) were collected for the purpose of revealing the high rate performance of electrode. The *Cs* values were calculated to be 1719.5 F/g at the small current density of 1 A/g based on equation (2), while the capacitance still retains 68.7% (1181.3 F/g) at 10 A/g. The remarkably capacitance characteristic derives from the synergistic effect of layered structure $Ni(OH)_2$/EG composite, which

greatly facilitate the rapid diffusion of ions to access the $Ni(OH)_2$ nanoparticles. The pore structures owing to embedding of nanoparticles are beneficial to the infiltration of electrolyte, Moreover, the $Ni(OH)_2$ nanoparticles homogeneously anchored on the interfacial interactions between the EG sheets and CNTs via *in-situ* electrodeposition, thus providing efficient transport of electrons across the interfaces for fast faradaic redox reactions to enhance capacitive performances [38].

The CV curves of AC electrode were shown in Fig. 6a, which presents a nearly rectangular shape and well maintained even at 20 mV/s. The result indicates that AC electrode have a typical double-layer capacitor behavior and fast electrolyte diffusion. The GCD curves with different current densities can be observed in Fig. 6b, showing a typical linear relationship between potential and time. The calculated *Cs* values of the electrode were 192.5, 173.7, 159.6, 152.2 F/g at 1, 2, 5, 10 A/g based on their discharge time, respectively.

3.3 Electrochemical performances of ASC device

The assembled ASC device can obtain a stable electrochemical voltage of 1.6 V according to CV curves with 2 mV/s scan rate (Fig. 7a). The mass ratio of two electrodes was decided according to the following formula:

$$m_+/m_- = Cs_- \times \Delta V_- / Cs_+ \times \Delta V_+ \qquad (5)$$

Where m (g), Cs (F/g), ΔV (V) represents the mass of electrode materials, specific capacitance and potential change in charge and discharge process, respectively. From Fig. 7b, the *Cs* of both negative and positive electrodes was obtained by discharge curves. The mass loading of negative electrodes was 15.0 mg/cm^2 according to the mass loading of positive electrode.

Fig. 8a represents the schematic illustration of the assembled ASC, two electrode materials and diaphragm is stacked into a sandwich-like structure. The CV curves of assembled ACS with various scan

rates (5~ 60 mV/s) can be obtain from Fig. 8b, indicating a collective contribution of double-layer capacitor behavior and pseudocapacitance. Besides, the CV profiles were nearly rectangular and symmetric even when the scan rate reach up to 60 mV/s, indicating a high rate capacity of the as-constructed ASC [39]. As can be seen from Fig. 8c, the GCD profiles of ASC with different current densities show asymmetric triangle pattern, revealing high coulombic efficiency and efficient capacitive behavior. The *Cs* based on discharge curves was calculated according to equation (2). As shown in Fig. 8d, the ACS can deliver a *Cs* of 64.6, 57.7, 50.5, 41.1, and 32.5 F/g at 0.5, 1, 2, 5, 10 A/g based on the toll mass of two electrodes, respectively. The high rate performance with 60% capacitance retention was obtained with increasing of current density (0.5 ~ 10 A/g). It is worth noting that an outstanding energy density (32.3 Wh/kg) can be obtained when the power density reach to 504.7 W/kg based on the equation (3) and (4). In addition, the assembled ACS can light up a red LED lamp (Fig. 8d inset).

The cycle stability of ASC was also evaluated by GCD test (5 A/g) for 1000 cycles. Fig. 9a shows that 79% of its initial capacitance is maintained. The result presents an excellent stability of assembled ASC. Fig. 9b shows Nyquist plots of assembled ASC, which consisted of a semi-circle arcs and straight line. The contact/electrolyte resistance (R_s) values are approximately 0.16 Ω and 0.18 Ω before and after cycling, respectively, demonstrating increasing of the ohmic resistance after 1000 cycles. Besides, the diameter of the semi-circle significantly increased, indicating a higher charge-transfer resistance (R_{ct}) because of collapsing of part of electro-active materials during the harsh redox reaction, which also affect the cycle stability of the ACS [40, 41]. In addition, slope of the straight line does not change too much after cycling, reveling an ideal capacitor behavior. All results show that the ASC device can demonstrate superior electrochemical performances.

4. Conclusions

In conclusion, Low cost EG can be used as an effective carbon support, a facile *in-situ* electrodeposited method has been adopted to synthesize a layered $Ni(OH)_2$/EG composite electrode, demonstrating satisfactory initial *Cs* of 1719.5 F g^{-1} at 1 A/g, remarkable rate capability (1181.3 F/g at 10 A/g). The high capacitive performances primarily derives from the synergistic effect of the layered $Ni(OH)_2$/EG composite. Furthermore, the assembled AC//$Ni(OH)_2$/EG device can deliver a prominent energy density of 32.3 Wh/kg at power density 504.7 W/kg, long cycling lifespan with 79% original capacitance after 1000 cycles. These results indicate that the facile synthesized high-performance $Ni(OH)_2$/expanded graphite electrodes could be applied for supercapacitor.

Acknowledgements

The support received from Education Department of Sichuan Province (13ZA0193), International Technology Collaboration of Chengdu Science and Technology Bureau, Scientific Research Foundation for Returned Scholars, Ministry of Education of China， Innovative Research Team of Southwest Petroleum University (2012XJZT002).

References

[1] C.-H. Lai, M.-Y. Lu, L.-J. Chen, J. Mater. Chem., 22 (2012) 19-30.

[2] N.S. Lewis, Science, 315 (2007) 798-801.

[3] Y.-G. Guo, J.-S. Hu, L.-J. Wan, Adv. Mater., 20 (2008) 2878-2887.

[4] P. Simon, Y. Gogotsi, Nat. Mater., 7 (2008) 845-854.

[5] M. Winter, R.J. Brodd, Chem. Rev., 104 (2004) 4245-4270.

[6] G. Wang, L. Zhang, J. Zhang, Chem. Soc. Rev., 41 (2012) 797-828.

[7] Y. Wang, Y. Song, Y. Xia, Chem. Soc. Rev., 45 (2016) 5925-5950.

[8] D.P. Dubal, O. Ayyad, V. Ruiz, P. Gomez-Romero, Chem. Soc. Rev., 44 (2015) 1777-1790.

[9] T. Ramesh, R. Jayashree, P.V. Kamath, S. Rodrigues, A. Shukla, J. Power Sources, 104 (2002) 295-298.

[10] J. Yan, Z. Fan, W. Sun, G. Ning, T. Wei, Q. Zhang, R. Zhang, L. Zhi, F. Wei, Adv. Funct. Mater., 22 (2012) 2632-2641.

[11] J. Ji, L.L. Zhang, H. Ji, Y. Li, X. Zhao, X. Bai, X. Fan, F. Zhang, R.S. Ruoff, ACS nano, 7 (2013) 6237-6243.

[12] X. Ma, Y. Li, Z. Wen, F. Gao, C. Liang, R. Che, ACS Appl. Mater. Interfaces, 7 (2015) 974-979.

[13] J.H. Park, O.O. Park, K.H. Shin, C.S. Jin, J.H. Kim, Electrochem. Solid-State Lett., 5 (2002) H7-H10.

[14] Q. Huang, X. Wang, J. Li, C. Dai, S. Gamboa, P. Sebastian, J. Power Sources, 164 (2007) 425-429.

[15] M.-H. Kim, J.-W. Lee, S.-M. Park, K.C. Roh,J. Ceram. Process Res., Vol. 13, Special, 2, pp. s265~s269 (2012).

[16] V.V. Obreja, Physica E, 40 (2008) 2596-2605.

[17] Z. Tang, C.h. Tang, H. Gong, Adv. Funct. Mater., 22 (2012) 1272-1278.

[18] L.L. Zhang, Z. Xiong, X. Zhao, J. Power Sources, 222 (2013) 326-332.

[19] R.R. Salunkhe, J. Lin, V. Malgras, S.X. Dou, J.H. Kim, Y. Yamauchi, Nano Energy, 11 (2015) 211-218.

[20] H. Wang, Y. Liang, T. Mirfakhrai, Z. Chen, H.S. Casalongue, H. Dai, Nano Res., 4 (2011) 729-736.

[21] Y. Liu, R. Wang, X. Yan, Sci.Rep., 5 (2015).

[22] L. Mao, C. Guan, X. Huang, Q. Ke, Y. Zhang, J. Wang, Electrochim. Acta, 196 (2016) 653-660.

[23] L. Wang, X. Li, T. Guo, X. Yan, B.K. Tay, Int. J. Hydrogen Energy, 39 (2014) 7876-7884.

[24] H. Wang, H.S. Casalongue, Y. Liang, H. Dai, J. Am. Chem. Soc., 132 (2010) 7472-7477.

[25] J. Kim, Y. Kim, S.-J. Park, Y. Jung, S. Kim, J. Ind. Eng. Chem., 36 (2016) 139-146.

[26] J. Xu, X. Gu, J. Cao, W. Wang, Z. Chen, J. SolidState Electrochem., 16 (2012) 2667-2674.

[27] L. Sui, S. Tang, Z. Dai, Z. Zhu, H. Huangfu, X. Qin, Y. Deng, G.M. Haarberg, New J. Chem., 39 (2015) 9363-9371.

[28] X. Wang, J. Liu, Y. Wang, C. Zhao, W. Zheng, Mater. Res. Bull., 52 (2014) 89-95.

[29] L. Sui, S. Tang, Y. Chen, Z. Dai, H. Huangfu, Z. Zhu, X. Qin, Y. Deng, G.M. Haarberg, Electrochim. Acta, 182 (2015) 1159-1165.

[30] Y. Bai, W. Wang, R. Wang, J. Sun, L. Gao, J. Mater. Chem. A, 3 (2015) 12530-12538.

[31] B.H. Ka, S.M. Oh, J. Electrochem. Soc., 155 (2008) A685.

[32] C. Guo, C. Wang, Compos. Sci. Technol., 67 (2007) 1747-1750.

[33] G. Helen Annal Therese and P. Vishnu Kamath, Chem.Mater., 2000, 12, 1195-1204..

[34] M. Taibi, S. Ammar, N. Jouini, F. Fiévet, P. Molinié, M. Drillon, J. Mater. Chem., 12 (2002) 3238-3244.

[35] Y. Ren, L. Gao, J. Am. Ceram. Soc., 93 (2010) 3560-3564.

[36] Y. Li, J. Yao, Y. Zhu, Z. Zou, H. Wang, J. Power Sources, 203 (2012) 177-183.

[37] L. Wang, X. Li, T. Guo, X. Yan, B.K. Tay, Int. J. Hydrogen Energy, 39 (2014) 7876-7884.

[38] L. Zhang, Q. Ding, Y. Huang, H. Gu, Y.E. Miao, T. Liu, ACS Appl. Mater.Interfaces, 7 (2015) 22669-22677.

[39] H. Ma, J. He, D.B. Xiong, J. Wu, Q. Li, V. Dravid, Y. Zhao, ACS Appl. Mater. Interfaces, 8 (2016) 1992-2000.

[40] Y. Xu, L. Wang, P. Cao, C. Cai, Y. Fu, X. Ma, J. Power Sources, 306 (2016) 742-752.

[41] Y. Zhao, L. Hu, S. Zhao, L. Wu, Adv. Funct. Mater., 26 (2016) 4085-4093.

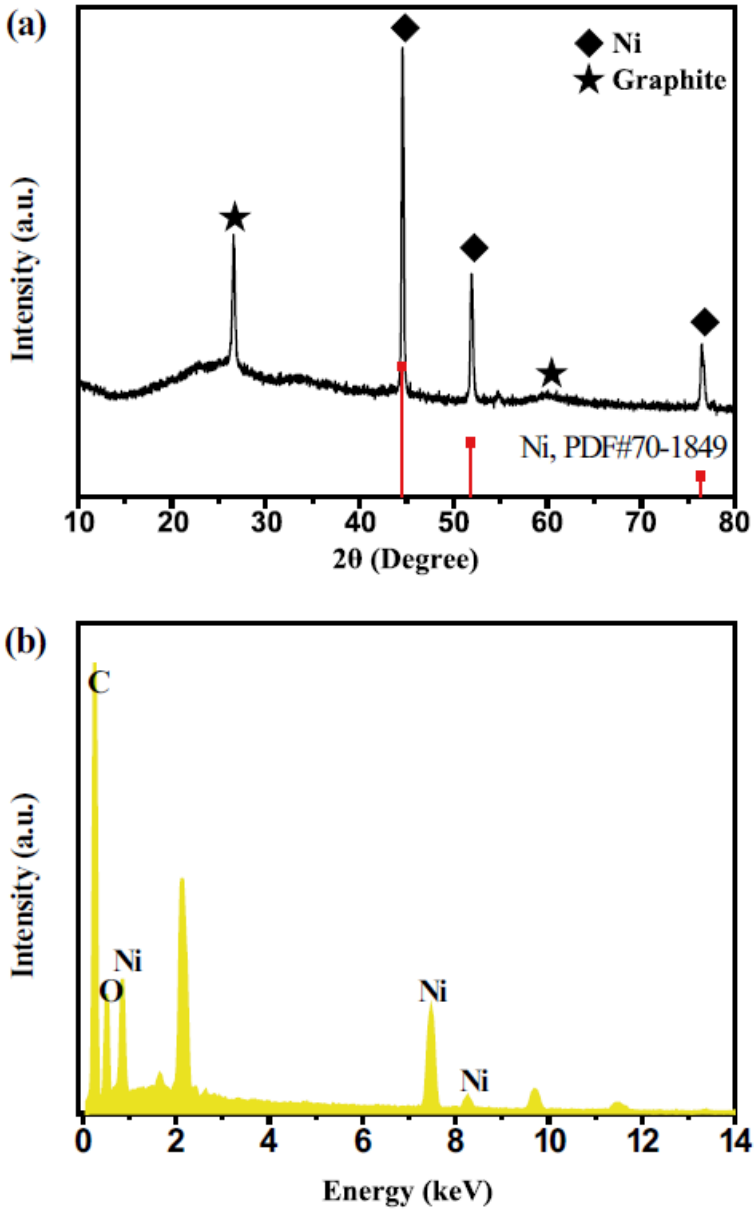

Fig. 1 **a** XRD patterns and **b** EDS spectra of $Ni(OH)_2$/EG composite

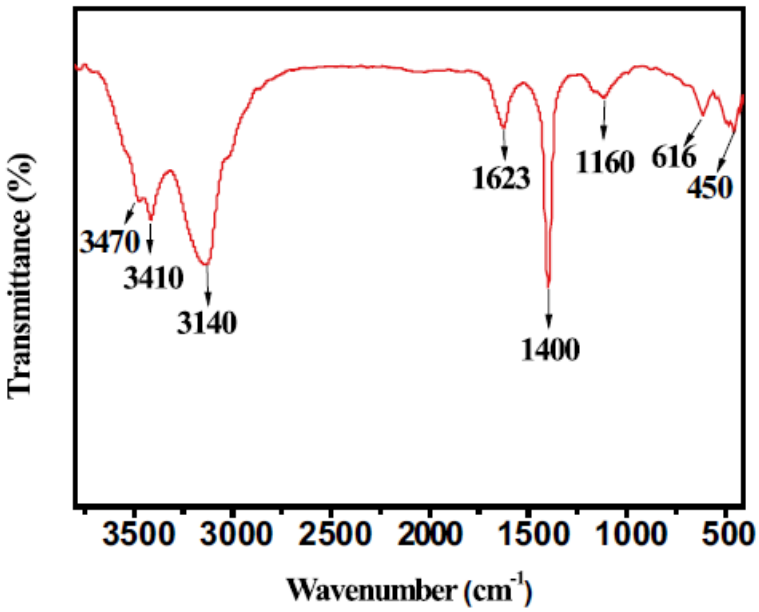

Fig. 2 FT-TR spectra of $Ni(OH)_2$/EG composite

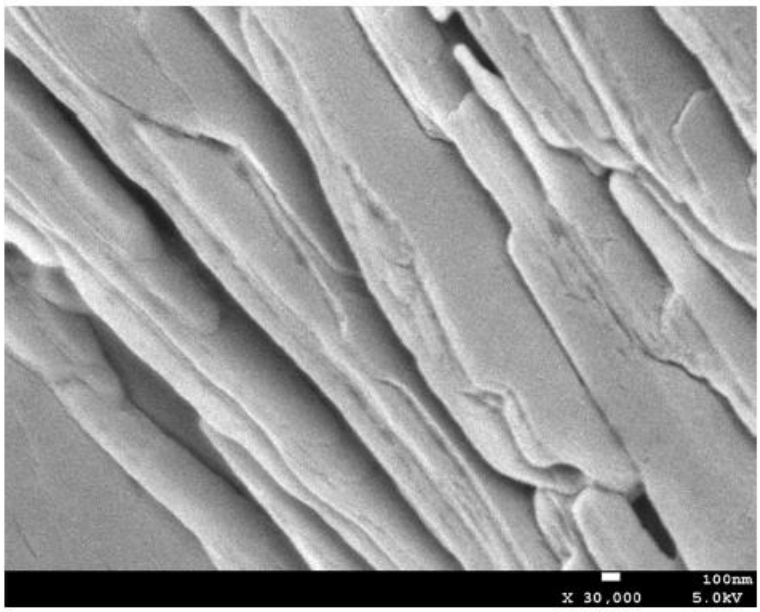

Fig. 3 FESEM image of expanded graphite

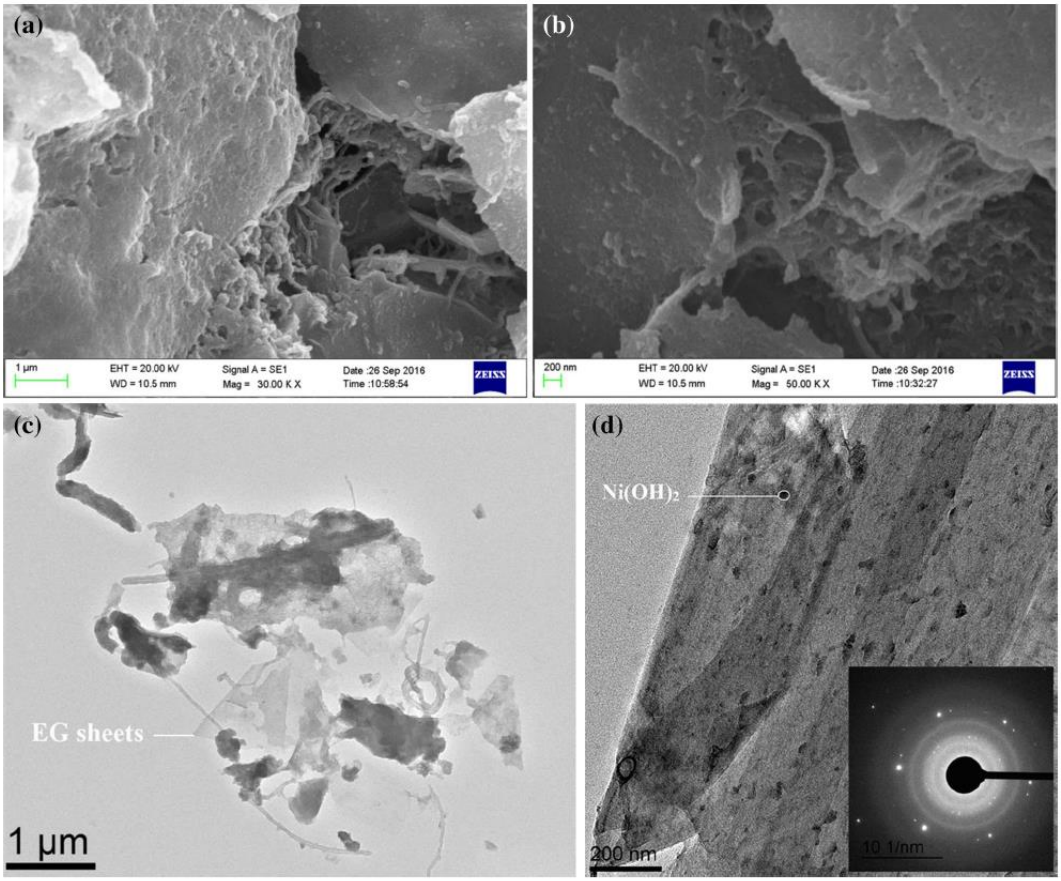

Fig. 4 SEM (**a, b**) and TEM (**c, d**) images of $Ni(OH)_2$/EG composite. Inset image shows selected-area electron diffraction pattern

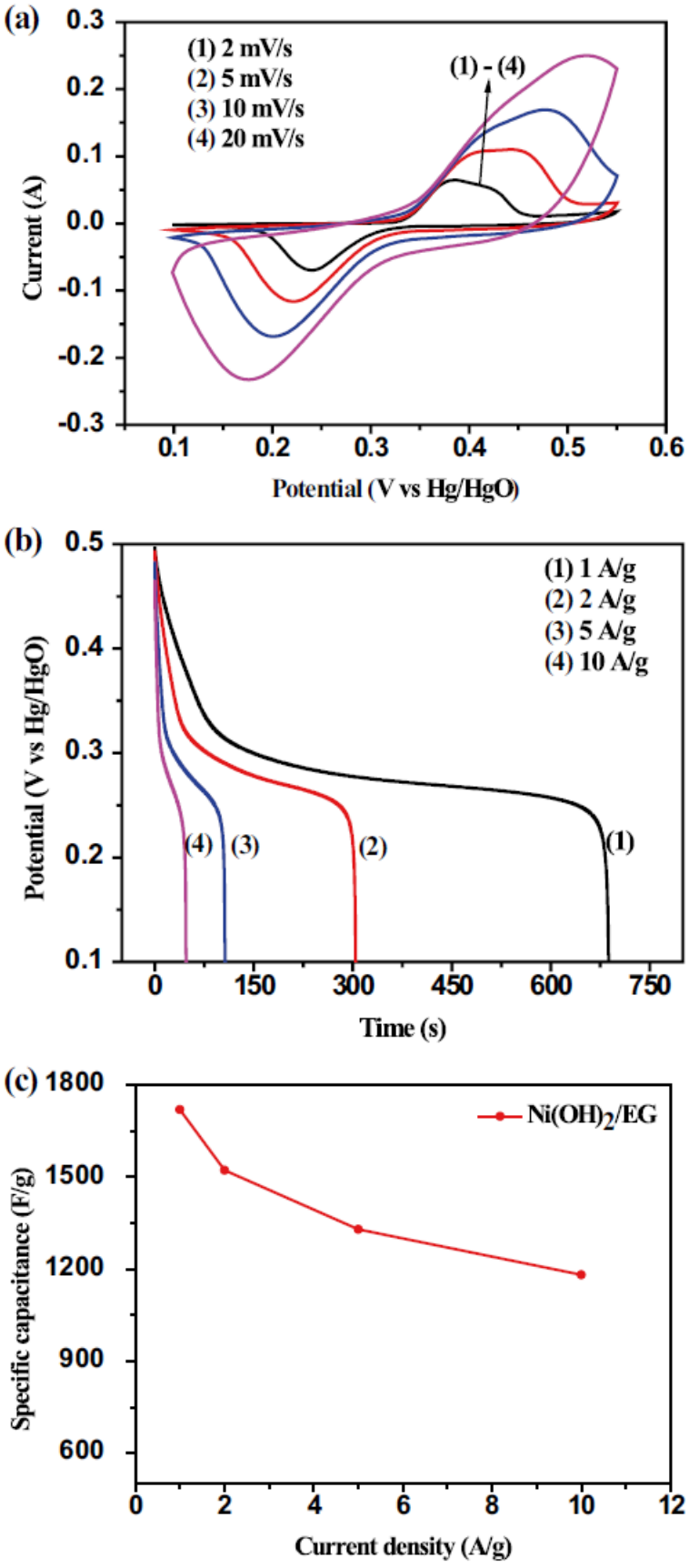

Fig. 5 **a** CV *curves* of $Ni(OH)_2$/EG composite electrode at various scan rates. **b** galvanostatic discharge curves at different current densities and **c** corresponding specific capacitance of $Ni(OH)_2$/EG composite electrode as a function of current densities

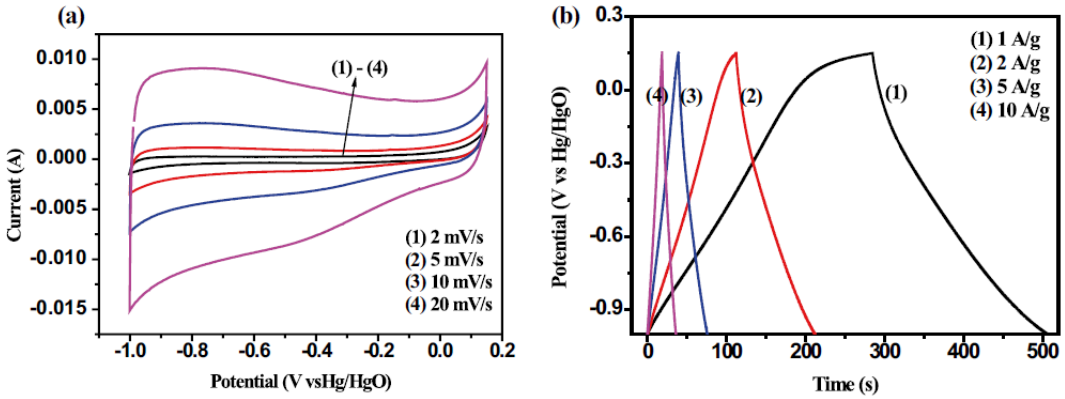

Fig. 6 **a** CV *curves* at various scan rates and **b** GCD *curves* at different current densities of AC electrode

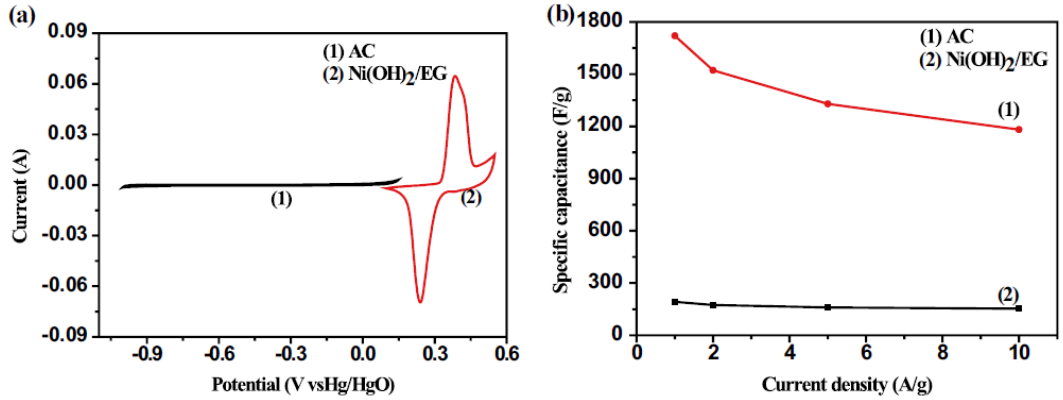

Fig. 7 **a** CV *curves* of AC and $Ni(OH)_2$/EG composite electrode at scan rate of 2 mV/s. **b** Specific capacitances of AC and $Ni(OH)_2$/EG composite electrode at various current densities

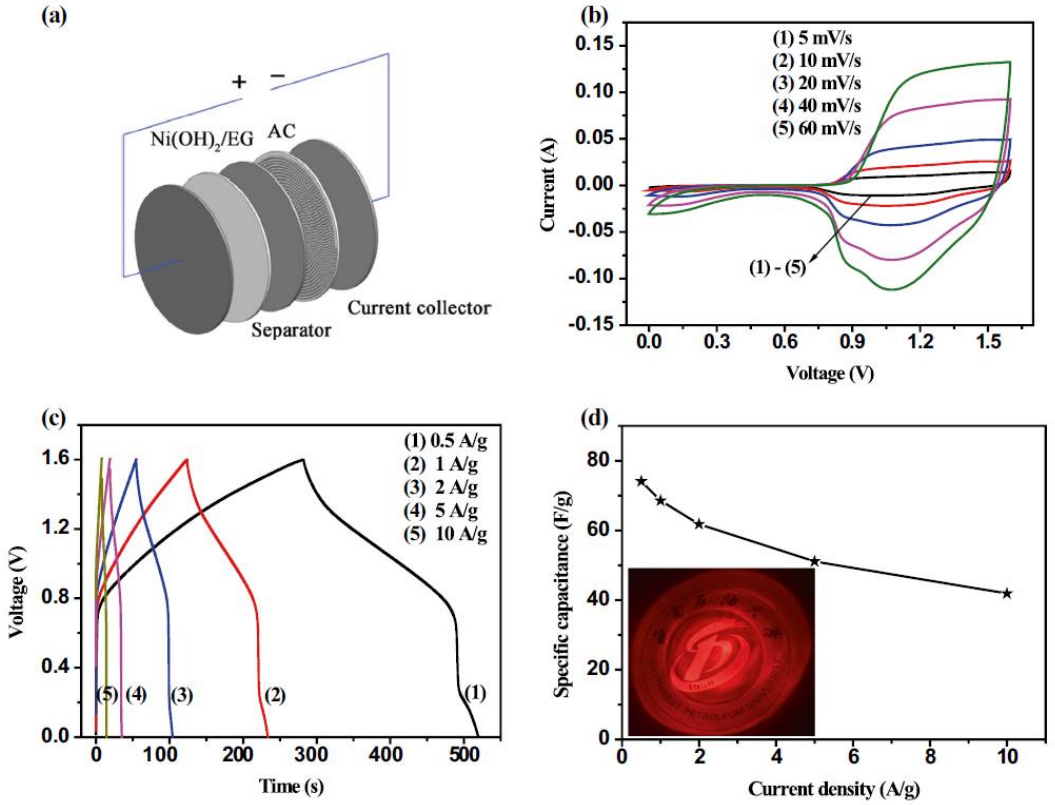

Fig. 8 **a** Schematic of the asymmetric supercapacitor (ASC) device composed of the $Ni(OH)_2$/EG composite and AC electrodes. **b** CV *curves* of the ASC device at different scan rates. **c** GCD *curves* at different current densities of the ASC device. **d** Specific capacitances of the ASC device at various current densities. *Inset* image shows LED lamp

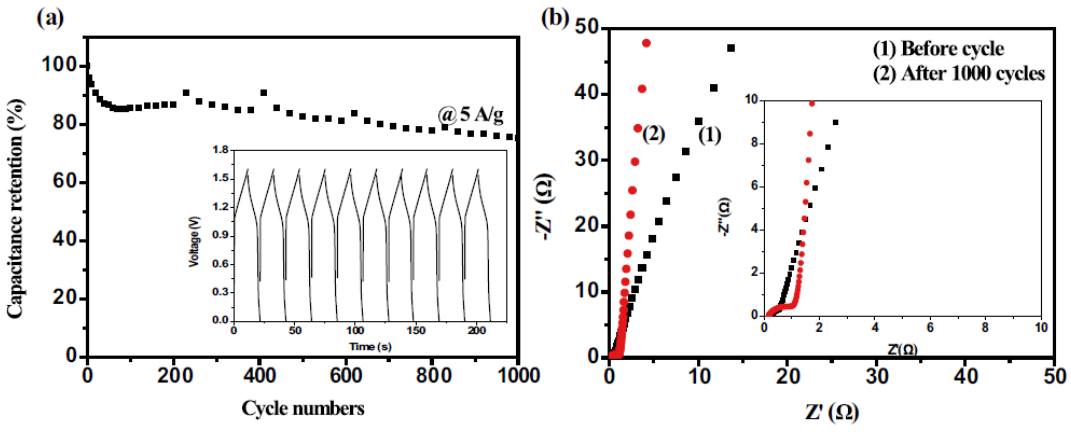

Fig. 9 **a** Cycle performance of the ASC device at current density of 5 A/g. *Inset* image shows the galvanostatic charge–discharge cyclic *curves* of the last 10 cycles. **b** Nyquist plots of EIS before and after 1000 cycles. The *inset* shows the impedance at high frequency region